Effects of chock and shock save effect on aerodynamic load and temperature of subsonic vacuum tube maglev train

Bin LIU*; Lei ZHANG; Yu LIU; Xia LI;

CRRC Tangshan Co., ltd., Tangshan Hebei China, 064000,

Abstract

The investigation of the impacts of congestion and shock wave effects on the aerodynamic loads and temperature of the vehicle body surface is of paramount significance for the engineering design and practice of subsonic vacuum tube transportation systems. Based on the Sutherland viscosity formula and the SST turbulence model, a three-dimensional numerical model is employed in this paper to simulate the aerodynamic characteristics of the tube train at different vacuum levels within the speed range of 700 to 1200 km/h. The accuracy of the numerical method is verified through the SOCBT model wind tunnel experiment. Through simulation analysis, the influence during the train's operation within the tube is explored. The results demonstrate that the influence trends of different vacuum levels on the temperature and pressure of the vehicle body surface remain unchanged. Furthermore, as the operating speed increases, after surpassing the critical Mach number, the degree of congestion within the tube aggravates with the increase in speed, and the influence trends on the temperature and pressure of the vehicle body surface are consistent. The pressure and temperature at the stagnation point of the train's head gradually decrease to the straight section. Due to the influence of oblique shock waves, the pressure and temperature slightly rise. At the rear car, the pressure and temperature significantly decrease due to the influence of supersonic expansion. At the nose of the rear car, the pressure and temperature increase as a result of the shock waves. The maximum surface temperature of the vehicle body emerges at approximately 350 K in the operating environment of 0.005 atm, while the maximum aerodynamic load is approximately 180 kPa in the normal pressure operating environment.

Keywords: Vacuum tube maglev train; Flow field characteristics; Shock wave effect; Choking; Aerodynamic load

1. Introduction

As an efficient and fast new mode of transportation, vacuum pipeline transportation system is gradually attracting wide attention. With the continuous increase of the running speed, the flow field structure in the

*Corresponding Author, Bin LIU 36676502@qq.com

pipeline becomes more and more complex, and there may be congestion phenomenon and shock wave effect, which significantly affect the aerodynamic load and temperature distribution on the surface of the vehicle body, and then have an important influence on the strength design of the vehicle body and the selection of materials. Therefore, it is very important for the design and engineering practice of vacuum tube train to analyze the influence of congestion and shock wave effect on the aerodynamic load and temperature of the body surface.

Since 2005, when Academician Shen Zhiyun systematically demonstrated the necessity and feasibility of vacuum pipeline high-speed transportation in China, relevant research has progressively deepened. In 2013, the Hyperloop concept introduced by SpaceX further propelled vacuum pipe maglev technology into the realm of engineering exploration, highlighting aerodynamic performance as the core challenge for system design [1]. TAYLOR et al. [2] conducted a comprehensive analysis of the Hyperloop system from both feasibility and economic perspectives. KIM et al. [3] investigated the aerodynamic characteristics of vacuum pipeline trains under varying operating speeds, vacuum levels, and blockage ratios, identifying critical speeds that could trigger shock waves at different pressures and blockage ratios. Liu Jali et al. [4] employed a three-dimensional compressible model to examine the relationship between the thermal effects of vacuum pipeline trains and factors such as train speed, blockage ratio, and pipeline pressure. Chen Yucheng et al. [5] analyzed the flow field structure in the wake region under different inlet Mach numbers using large eddy simulation turbulence models, offering significant engineering guidance for mitigating wake shocks and optimizing aerodynamic resistance.

Although many scholars at home and abroad have conducted extensive three-dimensional simulation analysis on the flow phenomenon of pipeline trains in recent years, few studies have paid attention to the effect of the flow phenomenon in the pipeline on the aerodynamic load and temperature of the train surface. This paper takes a vacuum tube maglev train system as the research object, and based on the shear stress transfer (SST) turbulence model, under the conditions of congestion ratio 0.178 and design speed of 700 km/h to 1200 km/h, the effects of shock effect, vacuum degree and different congestion degree on the train surface aerodynamic load and temperature are analyzed respectively. The aim is to provide theoretical basis for engineering design and practice.

2. Mathematical model

For vacuum tube maglev systems operating at speeds exceeding 400 km/h, where fluid velocities surpass 0.3 Mach, the flow characteristics exhibit significant complexity with substantial density variations. This necessitates the adoption of compressible gas as the simulation medium. The governing equations are expressed through the three-dimensional compressible Navier-Stokes equations in differential form:

$$\frac{\partial \rho}{\partial t}+\frac{\partial\left(\rho u_j\right)}{\partial x_j}=0 \tag{1}$$

$$\frac{\partial\left(\rho u_j\right)}{\partial t}+\frac{\partial\left(\rho u_i u_j\right)}{\partial x_j}=-\frac{\partial p}{\partial x_i}+\frac{\partial \tau_{ij}}{\partial x_j} \tag{2}$$

$$\frac{\partial(\rho e)}{\partial t}+\frac{\partial\left(\rho u_j h\right)}{\partial x_j}=div\left(K\text{grad}T\right)+\frac{\partial\left(u_i \tau_{ij}\right)}{\partial x_j} \tag{3}$$

*Corresponding Author, Bin LIU 36676502@qq.com

Equations (1) ~ (3) are continuity equation, momentum equation and energy equation respectively. Where, ρ is gas density; t is time; x_i、x_j is the cartesian component; u_i is the component of fluid velocity on u; p is for pressure; τ_{ij} is the viscous stress tensor; e is for internal energy; h is enthalpy; K is the heat conduction coefficient; T is the temperature.

3. Calculate the model

3.1. Geometric Model

The train model of the vacuum pipeline maglev system adopts the high-speed train model of three groups, as shown in Figure 1. The pipeline length is 87.4 m, the inner diameter is 3 m, the train height is 0.326 m, the length is 5 m. The center section model is shown in Figure 2.

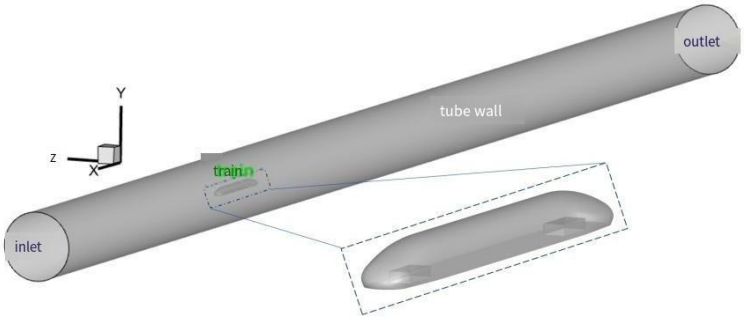

(a) Three-dimensional model

(b) Train body model

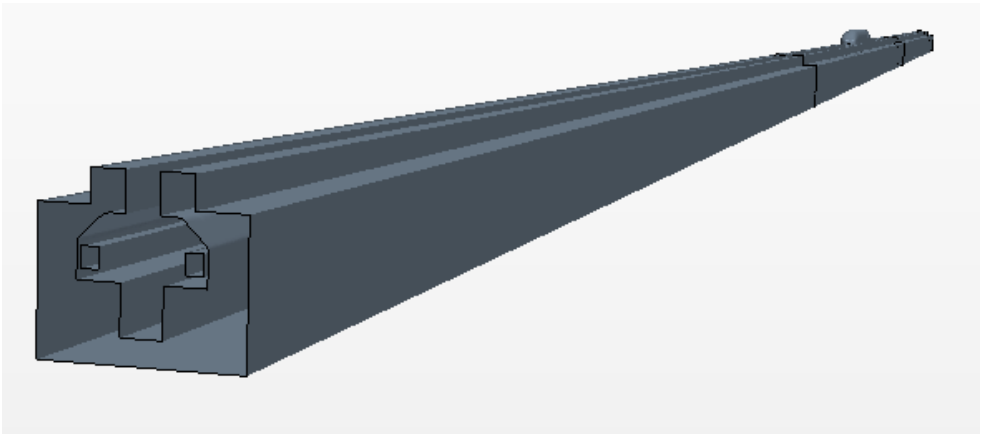

(c) Simplified model of bench end face

*Corresponding Author, Bin LIU 36676502@qq.com

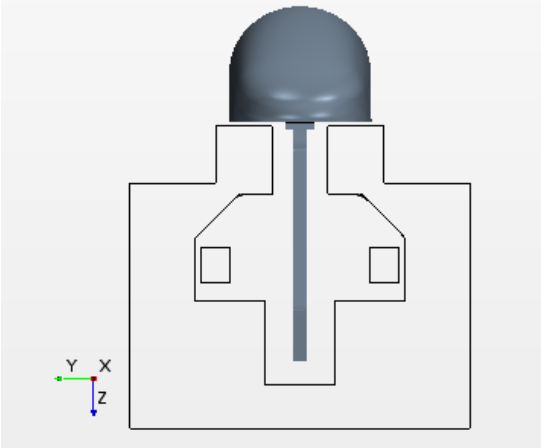

(d) Schematic diagram of the end face

Figure 1 3D model of vacuum tube train

3.2. Numerical Model

According to the fluid control equation, a three-dimensional calculation model of compressibility and viscosity is established. Considering the compressibility of gas, the coupled flow calculation method can effectively capture the compressibility characteristics of high-speed airflow. As the temperature increases, the viscosity of gas will increase, and the drastic compression of gas in the pipeline leads to obvious temperature changes. In order to more accurately describe the relationship between gas temperature and viscosity, Sutherland's law SST $k-\omega$ turbulence model can better capture the characteristics of the flow field near the wall of the train, and the computational solution accuracy is implicit second order.

The boundary conditions of the calculation area are set as follows: the pipeline adopts the viscous solid wall boundary, the entrance and exit of the pipeline adopts the far field boundary, the train surface is the viscous solid wall boundary, the initial ambient temperature is 288 K, the walls in the calculation domain are adiabatic conditions, that is, the heat exchange between the internal flow field and the external environment is not considered.

3.3. Calculation grid and independence verification

In order to effectively and quickly capture the characteristics of the flow field around the train, two layers of encryption area are set up for dimensional transition, which is divided into the middle encryption control body and the nearby encryption control body, as shown in Figure 2. According to different sizes y^+, the grid thickness and number of layers are set, and three sets of grids are divided into 25 million, 36 million and 45 million respectively.

*Corresponding Author, Bin LIU 36676502@qq.com

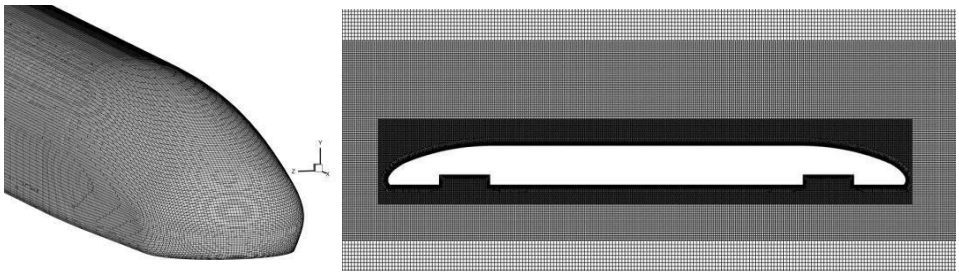

Figure 2 Grid division

The grid independence test was carried out when the operating speed was 400 km/h and the operating environment was 1atm, so as to eliminate the influence of grid size and number on the numerical results. As shown in Table 1, the aerodynamic resistance of the head/tail vehicle calculated by the three grid sets, the error of aerodynamic resistance of the head vehicle between the first grid and the second grid set is 1.1 %, and the error between the second grid and the third grid set is 1.7 %. Therefore, the second grid set has met the grid independence requirements, and this grid set is used in subsequent calculations.

Table 1 Grid independence test

Grid	Number of grids /10^4	Resistance / N	Relative error / %
1	2500	172	—
2	3600	174	1.1
3	4500	177	1.7

4. SCOBT model wind tunnel test validation

Considering the long and thin structure of vacuum tube train and the axisymmetric flow field structure, SOCBT projectile, which is formed by the combination of cut warhead, cylinder body and boat tail, is used as the verification object of the numerical calculation method. Kayser and Whiton completed a large number of experiments on SOCBT projectile in the 8-foot transonic wind tunnel of Langley Research Center [6]. Figure 3 shows the Socbt model and size, where D=0.057 m and the length of the front, middle and back segments are 3D, 2D and 1D, respectively.

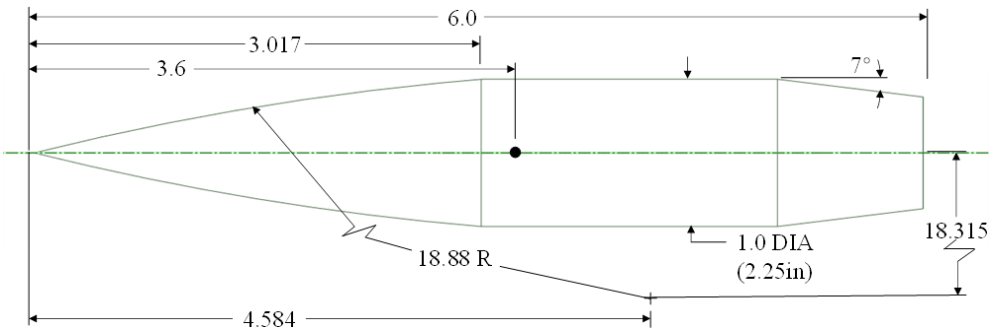

Figure 3 SOCBT model and size

In order to verify the reliability of the numerical method, the calculated boundary conditions are consistent with the experiment, assuming that the projectile does not move, the incoming flow Mach number is 0.91, the

*Corresponding Author, Bin LIU 36676502@qq.com

incoming flow Reynolds number is about, and there is no Angle of attack. 1.14×10^6 In order to better capture the flow field structure, mesh encryption is carried out around the model, the entrance and exit of the calculation domain are far field boundaries, the absolute pressure is 0.4atm, and the SST k-ω turbulence model is adopted.

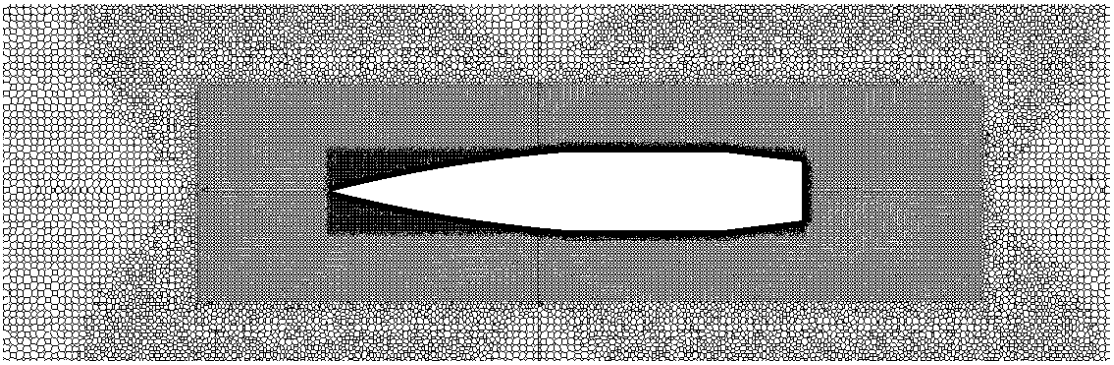

Figure 4 Longitudinal center section grid

In order to facilitate the comparison of simulation analysis results with experimental results and theoretical data, the pressure system number Cp is defined as

$$C_P = \frac{p - p_\infty}{0.5\rho_\infty v_\infty^2}$$

Where, p is the surface pressure of the projectile, and p_∞ ρ_∞ v_∞ are the pressure, density and velocity of the distant flow, respectively.

FIG 5 is the distribution diagram of projectile surface pressure coefficient. It can be seen that the calculated values are in good agreement with the experimental data and theoretical values, indicating that the grid generation strategy and numerical simulation method adopted can accurately calculate the aerodynamic characteristics of the vacuum pipeline train.

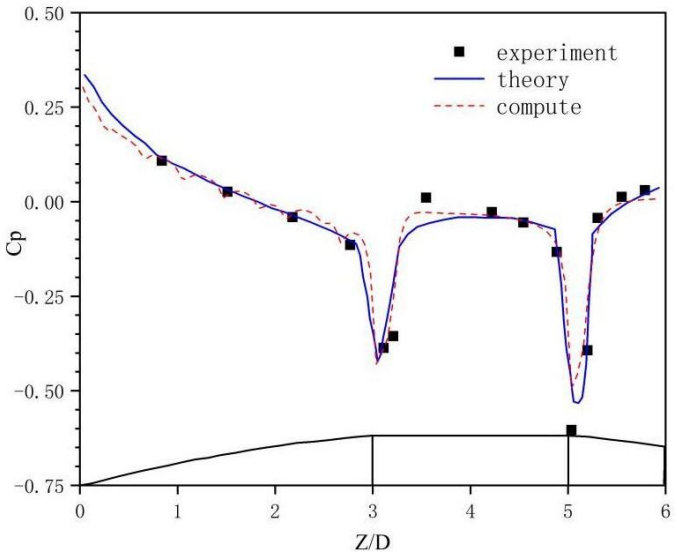

Figure 5 Distribution of surface pressure coefficient of the projectile

5. Calculation result

*Corresponding Author, Bin LIU 36676502@qq.com

Simulation analysis of the internal environmental pressure of the pipeline is 0.005 atm, 0.05 atm, 0.5 atm, 1atm (1 atm = 101325 Pa), and the running speed is 700 km/h, 1000 km/h, 1200 km/h, a total of 12 working conditions, as shown in Table 2.

Table 2 Combination table of calculation working conditions

Speed	700 km/h	1000 km/h	1200 km/h
Internal pressure of pipe	0.005 atm, 0.05 atm, 0.5 atm, 1 atm	0.005 atm, 0.05 atm, 0.5 atm, 1 atm	0.005 atm, 0.05 atm, 0.5 atm, 1 atm

According to the isentropic limit relation curve between the blocking ratio and the flow Mach number, it can be seen that the subsonic critical Mach number corresponding to the blocking ratio of 0.178 is 0.58, that is, when the train running speed reaches 710 km/h, there is congestion inside the pipeline. By comparing the flow field structure and congestion degree of pipeline train under different working conditions, the typical flow pattern of subsonic pipeline train flow is obtained.

5.1. Analysis of shock wave effect

FIG. 6 is the numerical Schlieren diagram of the central section of the pipeline train when the running speed is 1000 km/h and the ambient pressure is 1atm, which can give the waveform structure of the flow field more clearly and analyze the typical flow field under this working condition. FIG. 7 is the Mach number cloud diagram under this working condition.

According to the Mach number cloud map, it can be found that the incoming flow Mach number in front of the vehicle is between 0.4 and 0.5, which does not reach the Mach number 0.817 corresponding to the design speed of 1000 km/h, and it can be judged that the flow congestion occurs at this time. However, it can be seen from the numerical schlieren diagram that at the head of the vehicle, subsonic flow flows through the contraction and accelerates to the supersonic state, and an oblique shock wave is generated at the position of the vehicle body. The oblique shock wave is continuously reflected through the tube wall and the surface of the vehicle body. At the rear of the vehicle, the supersonic expansion flow causes a series of expansion waves to be generated, and at the end of the expansion wave, the flow converges to form an upper lip shock wave. After the wave flow, an obvious shear layer is formed, while a lambda-shaped shock wave is generated in the pipe, and then emitted between the pipe walls.

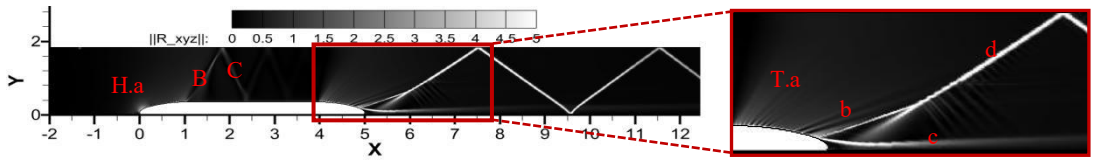

Figure 6 Numerical Schlieren diagram (1000 km/h, 1 atm) H: head car, T: tail car, H.a: subsonic accelerating flow, B: oblique shock wave, C: reflected shock wave, T.a: series of expansion waves, b: upper lip shock wave, c: shear layer, d: λ shaped shock wave

*Corresponding Author, Bin LIU 36676502@qq.com

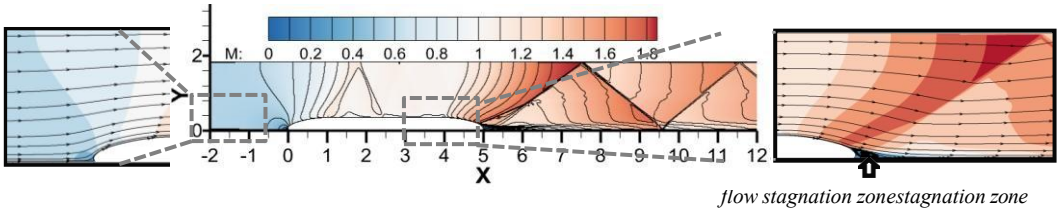

Figure 7 Mach number cloud image in the pipeline (1200 km/h, 1 atm)

FIG.8 shows the Mach number distribution curve of the body surface pressure, temperature and the middle section. It can be observed that the pressure and temperature of the body surface gradually decrease under the influence of the flow of subsonic acceleration at the front position, while the pressure and temperature of the body surface rise under the influence of oblique shock wave. The pressure and temperature distribution of the body surface are affected by the reflection of waves, resulting in fluctuating changes. At the rear of the car, affected by ultrasonic expansion, the surface pressure and temperature decreased, and at the rear of the car, affected by the shock wave of the upper lip, the pressure and temperature rose again, with the temperature increasing by about 50 %.

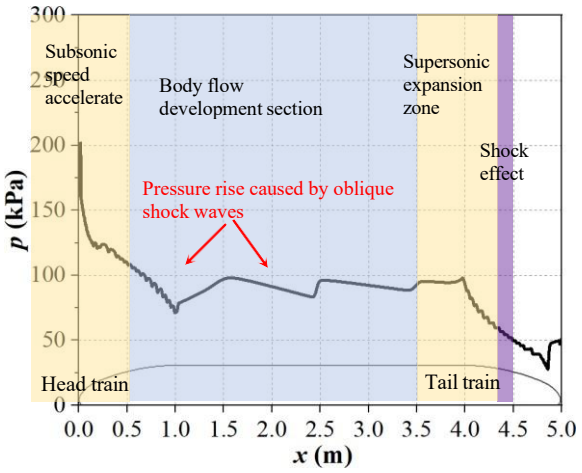

(a) Pressure curve

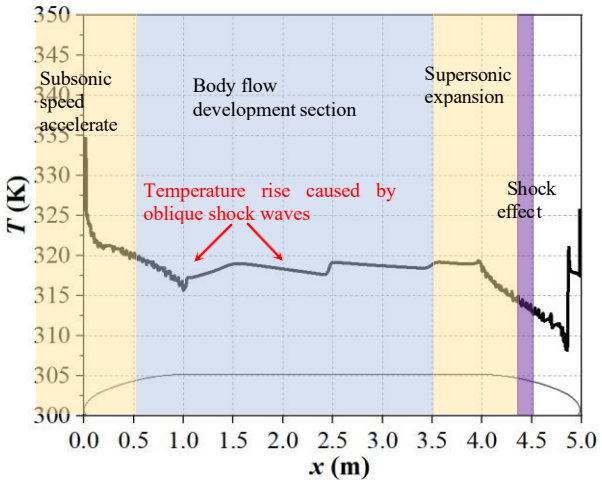

(b) Temperature curve

*Corresponding Author, Bin LIU 36676502@qq.com

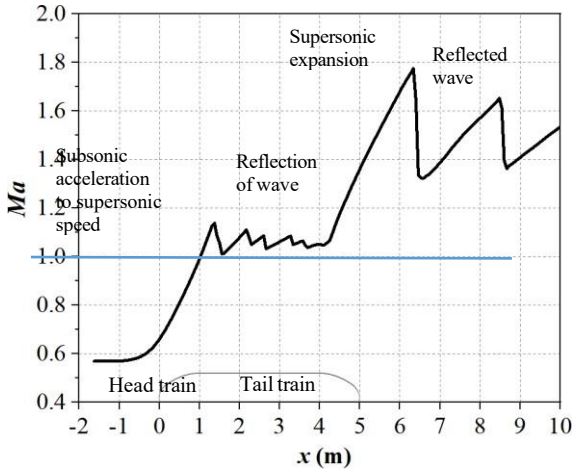

(c) centerline Mach number curve

Figure 8 Surface pressure, temperature and center-line Mach number distribution (1000km/h, 1atm)

5.2. 4.2 Influence of different vacuum degrees

FIG. 9 to FIG. 10 show the pressure coefficient and temperature distribution curves of the train surface under different vacuum degrees at the design speed of 1000 km/h. It can be seen from the figure that the variation trend of the surface pressure coefficient and temperature of the train body under different vacuum degrees at the same speed is basically the same. The influence of different vacuum degree on the pressure coefficient of the straight part of the car body is more obvious, and the influence on the temperature of the nose tip area of the rear car is greater. In fact, the pressure value of the car body surface is proportional to the vacuum degree, but it will not affect the dimensionless pressure coefficient, nor affect the flow field structure.

For the difference between the low vacuum condition and the normal pressure condition, it is because the wave system intensity on the body surface of the low vacuum degree is relatively weak, so the fluctuations of the body surface affected by the wave system are not obvious. Therefore, when the vacuum degree is 0.005 atm and 0.05 atm, the distribution of the surface pressure coefficient in the middle of the body does not change significantly. When the vacuum degree is 1 atm and 0.5 atm, the surface wave system of the car body is stronger, so the surface pressure coefficient changes more obviously.

As far as the surface temperature of the car body is concerned, when the air flow reaches the nose tip of the front car, the blockage ratio in the pipeline suddenly increases, resulting in an increase in the gas flow rate, and the surface temperature of the car body decreases to the flat section of the car body. Subsequently, because the blockage ratio does not change, the temperature change is not obvious, and the partial blockage ratio of the rear car flow line increases, and the surface temperature of the car body decreases. Until the temperature of the nose tip increases due to the influence of shock waves.

*Corresponding Author, Bin LIU 36676502@qq.com

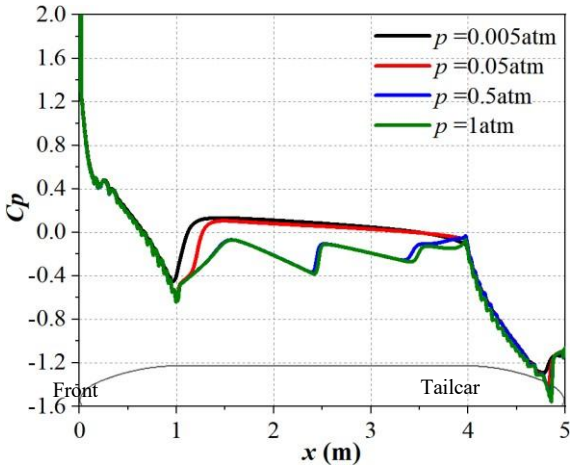

Figure 9 Surface pressure coefficient distribution of non-vacuum train (1000 km/h)

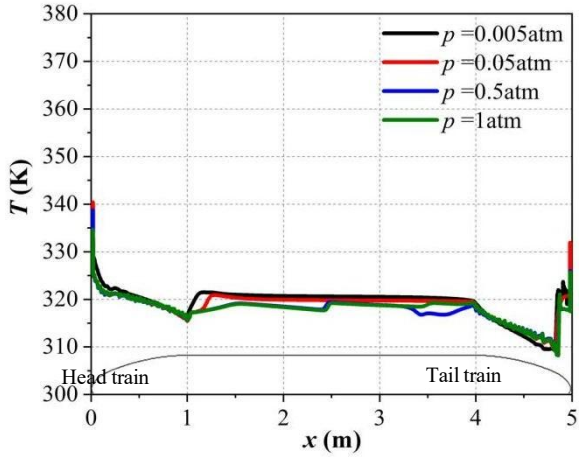

Figure 10 Surface temperature distribution of trains with different vacuum degrees (1000 km/h)

FIG. 11 is the 3D simulation result of the surface pressure and temperature of the train body under the design speed of 1000 km/h and the vacuum degree of 1atm; FIG. 12 is the pressure cloud image of the center section under different vacuum degrees at the operating speed of 1000 km/h; FIG. 13 is the column diagram of the maximum aerodynamic load on the surface of the train body. As can be seen from the results in FIG. 10, the temperature variation trend of the front car and the middle car is basically the same under the same speed and different vacuum degree. The temperature range of the car body surface is shown in Table 3. The surface pressure and pressure difference of the train under different vacuum degrees are shown in Table 4.

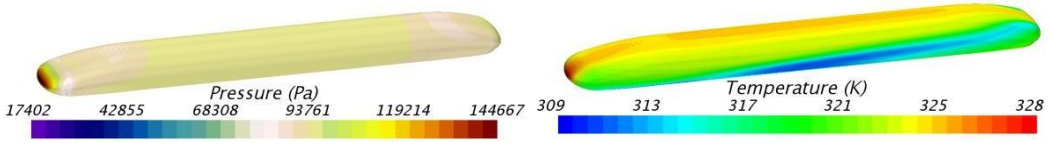

Figure 11 Distribution of pressure and temperature on the surface of the train body at 1000 km/h and 1 atm

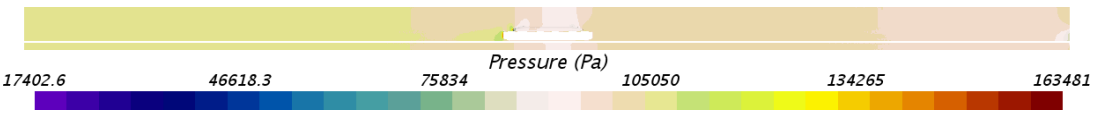

*Corresponding Author, Bin LIU 36676502@qq.com

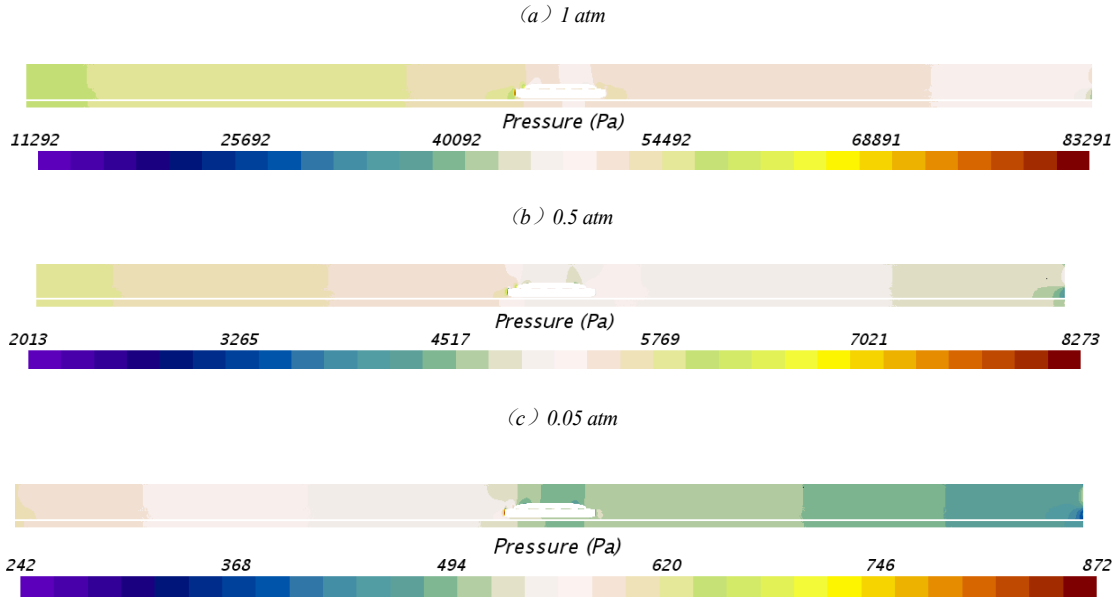

Figure 12 1000 km/h center cross section pressure

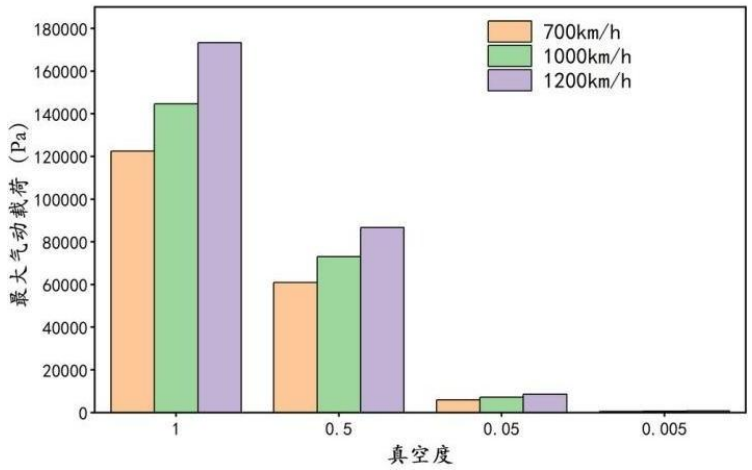

Figure 13 Maximum aerodynamic load on the body surface

The stagnation point pressure in the system appears at the nose tip of the nose, because the pressure in this area is greater than the surrounding pressure, so this part of the high-pressure medium diffuses to all directions around in the form of compression waves. Among them, part of the medium moves in the forward direction of the train, part of the medium moves in the opposite direction of the train forward, and this part of the medium is accelerated through the ring gap between the train and the pipeline in the process of moving to the rear, resulting in the pressure gradually reduced in the ring gap, reducing to the system pressure below, and finally at the exit of the ring gap. That is, due to the sudden increase of space near the forehead at the rear of the car, the nearby system pressure is minimized. At the rear of the train, on the one hand, the air flow in the annular gap escapes outward at a high speed and impacts in the opposite direction of the train. On the other hand, relative to the low pressure area of the annular gap, the normal pressure medium at the tail of the train moves along the direction of the train under the pressure difference. The two opposite air flows collide and fuse at the rear of the train,

*Corresponding Author, Bin LIU 36676502@qq.com

forming a low-pressure vortex that is slightly lower than the system pressure.

Table 3 Temperature range of vehicle body surface (K)

Vacuum degree /atm	Speed / km·h		
	700	1000	1200
1	296 ~ 307	309 ~ 328	322 ~ 346
0.5	297 ~ 307	311 ~ 329	332 ~ 353
0.05	288 ~ 306	286 ~ 329	290 ~ 343
0.005	297 ~ 356	264 ~ 331	333 ~ 346

Table 4 Body Surface Pressure range (Pa)

Vacuum degree / atm	700 km/h			1000 km/h			1200 km/h		
	Minimum pressure	Maximum pressure	Pressure Difference	Minimum pressure	Maximum pressure	Pressure Difference	Minimum pressure	Maximum pressure	Pressure Difference
1	33873	122141	88268	12773	144776	132003	11475	173460	161985
0.5	17310	60936	43626	9112	73186	64074	5798	86742	80944
0.05	2653	6007	3354	1633	7152	5519	1255	8671	7416
0.005	493	528	35	345	664	319	384	836	452

Table 5 Variation of stagnation point pressure and pressure difference in the pipeline

Vacuum degree / atm	1 ~ 0.5			0.5 ~ 0.05			0.05 ~ 0.005		
Operating speed / km·h	700	1000	1200	700	1000	1200	700	1000	1200
Stagnation pressure increase / Pa	61205	71590	86718	54929	66034	78071	5479	6488	7835
Ratio	120.81%	141.31%	171.17%	120.47%	144.82%	171.22%	120.16%	142.29%	171.83%
Minimum pressure reduction size / Pa	16563	3661	5677	14657	7479	4543	2160	1288	871
Scale	32.69 %	7.23 %	11.21 %	32.15 %	16.40 %	9.96 %	47.37 %	28.25 %	19.10 %
Pressure differential reduction size / Pa	44642	67929	81041	40272	58555	73528	3319	5200	6964
Scale	88.12 %	134.08 %	159.96 %	88.32 %	128.42 %	161.26 %	72.79 %	114.04 %	152.73 %

It can be seen from Table 5 that under the three operating speeds, when the vacuum degree in the tube decreases from 1atm to 0.5 atm, 0.5 atm to 0.05 atm, and 0.05 atm to 0.005 atm, the increase of stagnation point pressure is the same; When the vacuum degree is reduced from 0.05 atm to 0.005 atm, the minimum pressure reduction

*Corresponding Author, Bin LIU 36676502@qq.com

ratio increases significantly, about 11 % ~20 %, and the higher the speed, the greater the reduction ratio, while the pressure difference reduction ratio decreases, about 1 %~4 %, and the higher the speed, the smaller the reduction ratio.

5.3. 4.3 Influence of the degree of congestion

FIG. 14 shows the pressure distribution of the central section of the pipeline and the surface of the vehicle body at different running speeds when the vacuum degree is 1atm. The critical Mach number of subsonic choking limit corresponding to the congestion ratio in this paper is 0.58, that is, the design speed of 700 km/h is near the critical Mach number, while congestion will occur in the pipeline at the design speed of 1000 km/h and 1200 km/h, but the degree of congestion is different. At the sections of 1000 km/h and 1200 km/h, It can be clearly seen that the pressure change of the front end entrance section of the vehicle is obvious.

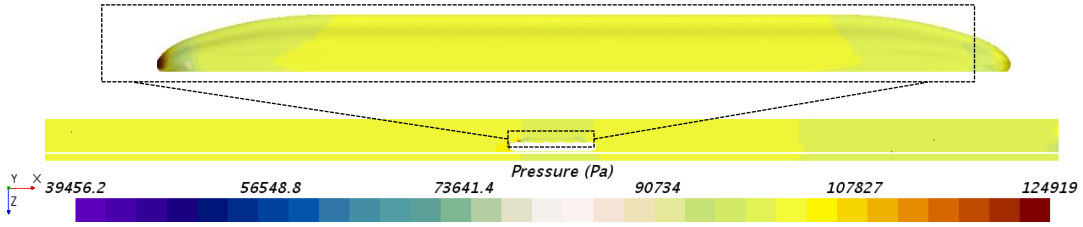

(a) 700 km/h

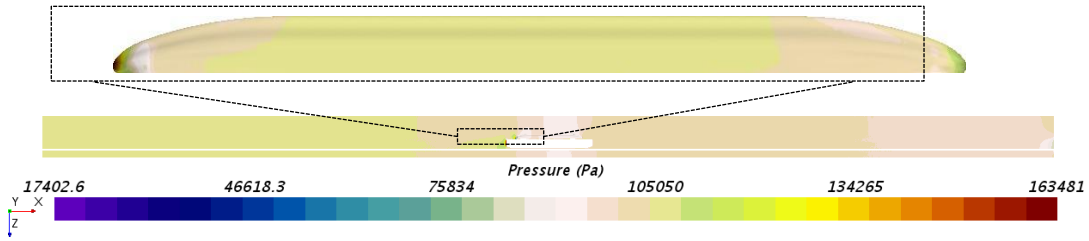

(b) 1000 km/h

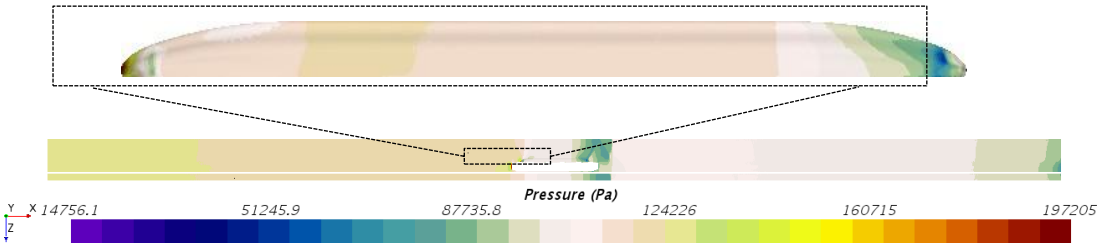

(c) 1200 km/h

Figure 14 Pressure distribution of pipeline center section and vehicle body surface at 1atm

FIG. 15 to FIG. 17 show the Mach number distribution curves of the surface pressure, temperature and corresponding center line of the train body at 3 different design speeds under 1 atmosphere pressure. It can be seen from the figure that the surface pressure and temperature of the train body are different under different design speeds. With the increase of congestion degree, the surface pressure and temperature of the train body

*Corresponding Author, Bin LIU 36676502@qq.com

will further increase, and the Mach number distribution law of the flow field under congestion condition is consistent.

Since the running speed of 1000 km/h and 1200 km/h are in the choked state, the pressure change trend of the body surface is the same. When the running speed of 1200 km/h is higher than that of 1000 km/h, the upper surface pressure of the body increases by about 8600 Pa, an increase of 9.1 %. The temperature change trend of the three speed levels is the same, and the temperature rise of the surface of the car body compared with the ambient temperature ΔT is 17.2 K, 33.2 K and 48.1 K, respectively.

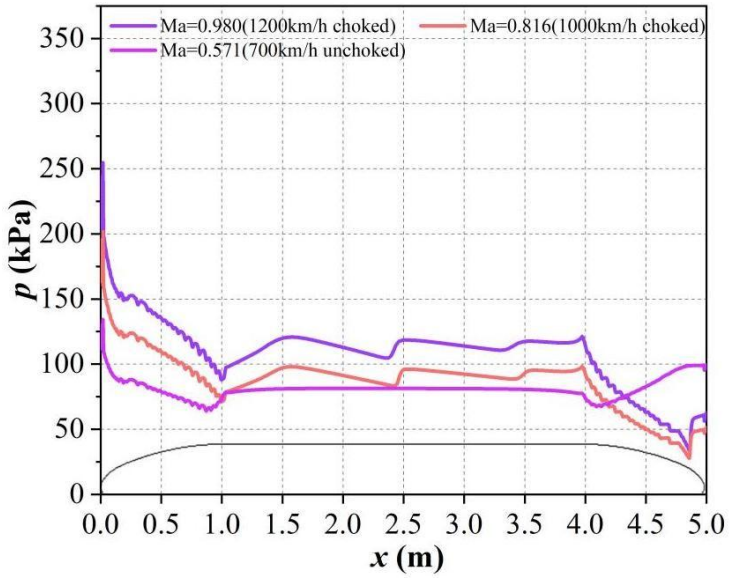

Figure 15 Surface pressure distribution of the vehicle body at different design speeds of 1 atm

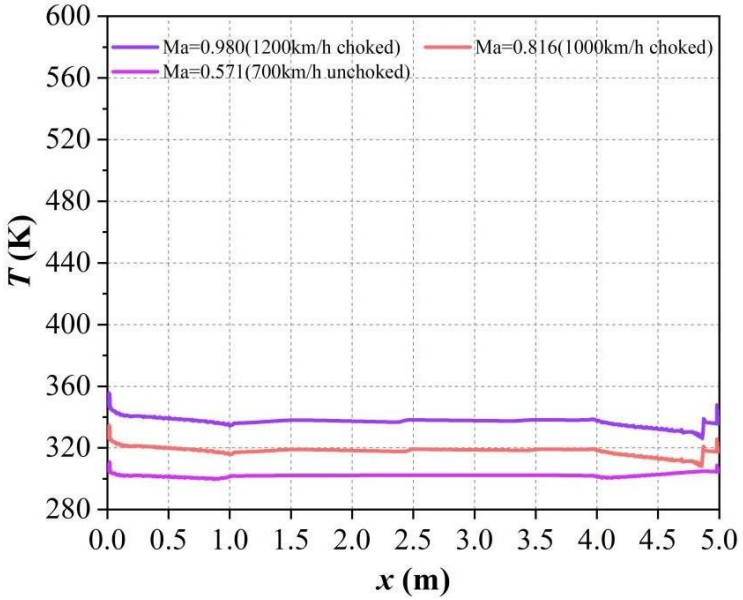

Figure 16 Temperature distribution of the upper surface of the car body at different design speeds of 1 atm

*Corresponding Author, Bin LIU 36676502@qq.com

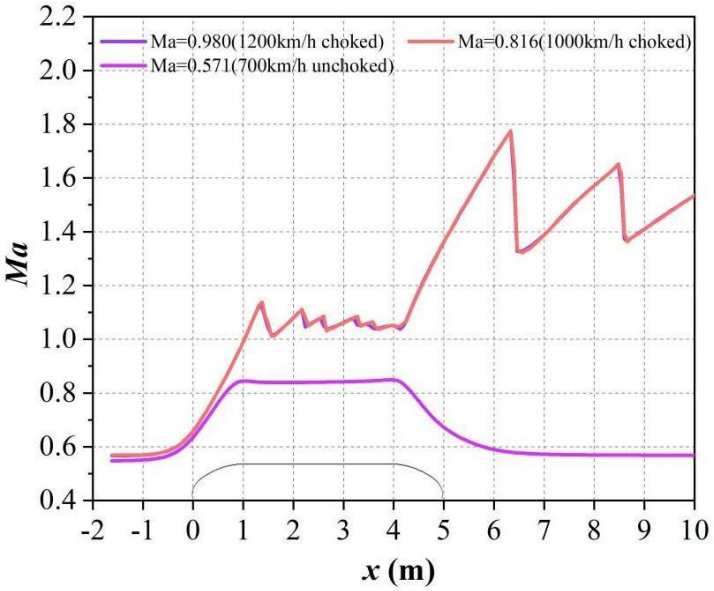

Figure 17 Mach number distribution in the car body and some pipes at different design speeds of 1 atm

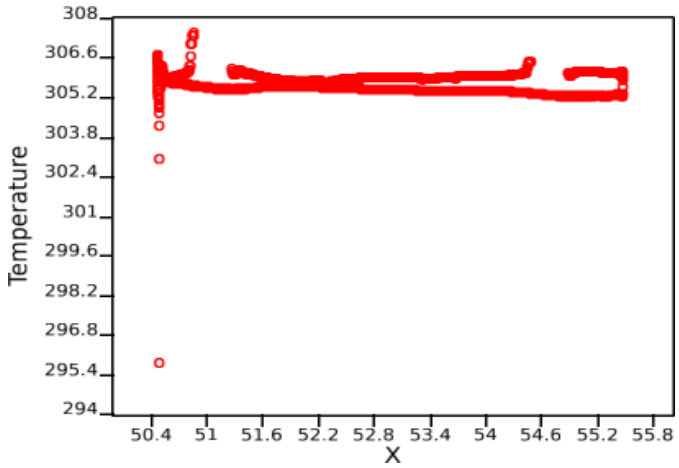

（a）700 km/h

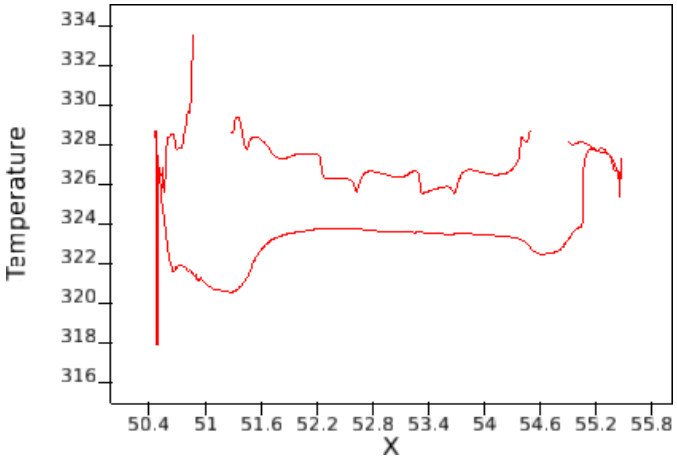

(b) 1000 km/h

*Corresponding Author, Bin LIU 36676502@qq.com

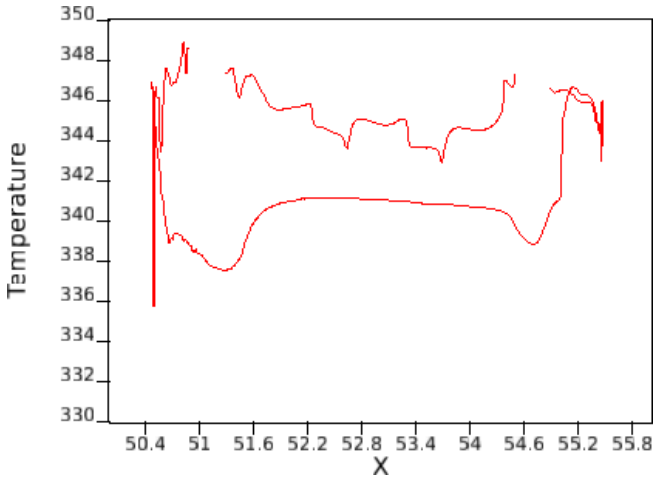

(c) 1200 km/h

Figure 18 Surface temperature distribution of 1atm body symmetry surface

FIG. 18 is the temperature distribution diagram of the symmetrical surface of the train body. The overall temperature of the bottom of the train is higher than that of the upper surface and side of the train. Due to the small annular gap space at the bottom, the airflow movement is blocked by the bottom, most of the kinetic energy is converted into heat energy, and the heat gathers in the bottom of the train to form a high-temperature area, so the temperature of the bottom flow field is higher than that of other areas. The temperature distribution trend of the upper and lower surfaces of the train at different speeds is basically the same. When the initial pressure and blockage ratio in the tube are constant, when the train runs at a lower speed, the airflow velocity through the annular gap between the train and the pipe is smaller, the friction resistance is smaller, and the pressure difference resistance of the front and rear cars is also smaller, so the energy consumed to maintain the running at this speed is also smaller. Therefore, the maximum internal temperature of the system does not change much; When the speed increases gradually, the air velocity along the head of the train through the annular gap between the train and the pipeline increases, and the friction resistance increases, which not only causes the collision and mixing of the air flow to intensify, but also causes more air to impact the inner wall of the pipeline with the direction of the train's locomotive flow line. While changing the direction of the air flow, most of the kinetic energy carried by the air flow is directly converted into heat. Increase the temperature of the whole system.

6. Conclusion

Through the analysis of the effects of shock wave, vacuum degree and pneumatic congestion on the surface temperature and aerodynamic load of subsonic vacuum tube train, the main conclusions are as follows:

(1) When the train runs in the vacuum pipeline at subsonic speed, the pressure distribution on the train surface is basically the same. The maximum pressure appears in the position of the stagnation point of the front, and gradually decreases along the direction of the length of the car. The pressure change is small in the flat section of the body. The minimum pressure appears in the junction between the shoulder and the roof of the rear car, not the nose tip.

*Corresponding Author, Bin LIU 36676502@qq.com

(2) When the train runs in the pipeline system with different vacuum degrees, increasing the vacuum degree in the pipeline will reduce the pressure in the pipeline system, which can effectively reduce the pressure difference resistance of the head and tail car, thus reducing the operation energy consumption of the train. When the train running speed increases from 700km/h to 1000km/h and 1200km/h, the system pressure difference gradually decreases with the reduction of the system pressure, and the reduction range is basically unchanged.

(3) The temperature at the head and tail of the train is high. Under a certain system pressure and running speed, the maximum temperature distribution law of the train surface is roughly the same. The shock wave has little influence on the temperature change of the head car and the middle car, mainly concentrated in the nose area of the rear car, and the temperature increases by about 50 %. Under the same system pressure, the temperature increases with the increase of the speed.

Reference

1. MUSK E. Hyperloop Alpha[R]. SpaceX, 2013, 13−14.

2. TAYLOR C L, HYDE D, BARR L, et al. Hyperloop commercial feasibility analysis: high level overview[R].United States Department of Transportation, 2016.

3. KIM T K, KIM K H, KWON H B. Aerodynamic characteristics of a tube train[J]. Journal of Wind Engineering and Industrial Aerodynamics, 2011, 99(12):1187−1196.

4. LIU Jiali, ZHAGN Jiye, ZHANG Weihua. Analysis of pneumatic characteristics of vacuum pipeline and high-speed train[J]. Journal of Mechanical Engineering, 2013, 49(22): 137−143.

5. CHEN Yucheng, QIN Bin, LIANG Xifeng. Three-dimension study on aerodynamics characteristics and shock wave effects of the vacuum tube train[J]. Jouranal of Railway Science and Engineering. 2023, 20(2): 412-422

6. KAYSER, L.D., WHITON, F., March 1982. Surface Pressure Measurements on a Boattailed Projectile Shape at Transonic Speeds. U.S. Army Ballistic Research Laboratory, ARBRL-MR-0316.

7. ZHOU Peng, LI Tian, ZHANG Jiye, et al. Research on shock wave trains generated by the hyper train in the evacuated tube[J]. Journal of Mechanical Engineering, 2020, 56(2): 86-97.

8. ZHOU Peng, LI Tian, ZHANG Jiye, et al. Aerothermal effect generated by hyper train in the evacuated tube[J]. Journal of Mechanical Engineering, 2020, 56(8): 190-199.

9. ZHANG Xiaohan, LI Tian, ZHANG Jiye, et al. Aerodynamic choked flow and shock wave phenomena of subsonic evacuated tube train[J]. Journal of Mechanical Engineering, 2021, 57(4): 182-190.

10. JIA Wenguang. THE CHARACTERISTIC INVESTIGATIoN oF EVACUATED TUBE TRANSPoRT SYSTEM oN THERMoDYNAMICS[D]. 2013, Qingdao University of Science and Technology.

11. Zhou Peng. STUDY ON AERODYNAMIC CHARACTERISTICS OF EVACUATED TUBE HIGH SPEED TRAIN][D].

*Corresponding Author, Bin LIU 36676502@qq.com

2017, Southwest Jiaotong University.

12. ZHANG Yinlong, WANG Xiaofei, ZHANG Kun, et al. Aerothermal Characteristics of Maglev Transportation in Evacuated Tube with Different Blocking Ratios[J]. 2022, 42(5):394-403.

13. JANG K S, LE T, KIM J, et al. Effects of compressible flow phenomena on aerodynamic characteristics in Hyperloop system[J]. Aerospace Science and Technology, 2021, 117(11): 106970.

14. LI T, SONG J Y, ZHANG X H, et al. Theoretical and numerical studies on compressible flow around a subsonic evacuated tube train[J]. Proceedings of The Institution of Mechanical Engineers Part C-Journal of Mechanical Engineering Science. https://doi.org/10.1177/09544062211072461.

15. ZHOU K Y, DING G F, WANG Y M, et al. Aeroheating and aerodynamic performance of a transonic hyperloop pod with radial gap and axial channel: A contrastive study[J]. Journal of Wind Engineering and Industrial Aerodynamics, 2021, 212: 104591.

16. BRAUN J, SOUSA J, PEKARDAN C. Aerodynamic design and analysis of the Hyperloop[J]. AIAA JOURNAL, 2017, 55: 4053-4060.

17. Wang Jukun，Bao Shijie，Hu Xiao，et a1．Numerical Study on the Influence of the Speed on the Aerodynamic Thermal in the HTS Maglev-Evacuated Tube Transpon System[J]. IEEE Transactions on Applied Superconductivity, 202l, 31(8): 0500804

*Corresponding Author, Bin LIU 36676502@qq.com